We are IntechOpen, the world's leading publisher of Open Access books Built by scientists, for scientists

6,700
Open access books available

180,000
International authors and editors

195M
Downloads

Our authors are among the

154
Countries delivered to

TOP 1%
most cited scientists

12.2%
Contributors from top 500 universities

Interested in publishing with us?
Contact book.department@intechopen.com

Numbers displayed above are based on latest data collected.
For more information visit www.intechopen.com

Chapter

Surface Microstructure Changes Induced by Ion Beam Irradiation

Carlos A. Camacho Olguín, Arturo García Bórquez,
Carlos A. González Rodríguez, Héctor Cruz Mejía
and Marco Solorio Ávila

Abstract

As a study result of irradiation-induced damage, various mathematical models have been developed to explain the phenomenon of irradiation-induced surface sputtering, these models are currently used in technological fields as diverse as materials characterization and in thin film deposition used in the manufacture of electronic or medical components. However, the phenomenon is not fully understood due to its high complexity, this work has the goal to present experimental evidence of the changes induced in the surface of hypereutectic alloy Ni-22% at Si promoted by the nickel ion beam irradiation, the surface changes induced will be explained in terms of the Sigmund theory of surface sputtering.

Keywords: ion beam irradiation, sputtering yield, surface microstructure, preferential sputtering, chemical and geometrical sputtering

1. Introduction

Material irradiation, material bombardment with energetic particles in the electro-volt to mega-electro-volt range, generally promotes changes in the material microstructure as a result of the energy transference between the solid atoms and the particle used to bombing the solid. The induced microstructural changes by ion beam irradiation that have been investigated and reported during the past five decades are: surface erosion, cratering, atoms implantation at controlled depth, crystal lattice disorder, phase transformations, second phases precipitation, etcetera [1, 2].

Because ion irradiation can deposit high energy densities locally in relatively short time periods, it could be used to evade thermodynamic constraints and create microstructures containing non-thermodynamic equilibrium phases [3, 4].

- When a surface is bombarded by an energetic ion beam a rich variety of surface structures are developed at atomic, microscopic, and macroscopic scales. These structures include elevations, with respect to the surrounding surface, e.g., plateaus,

cones, and pyramids among others, depressions, e.g., pores and cavities. These features may occur singly or in large numbers and often form repetitive patterns.

- The irradiation process induces the mass transport phenomenon as a result of the point defect formation and their posterior annihilation in point defect sinks [5]. In binary alloys characterized by solute-defect complexes formation with strong interactions, for example, Cu-Be and Ni-Si, a few point defects are required to transport a solute atom considerable distance, and dramatic changes in solute distribution would occur [6].

- It is known that the irradiation promoted the second phase's formation under conditions of temperature and solute concentration that thermodynamically do not correspond to their stability field. The non-equilibrium second phase formation is promoted by irradiation-induced segregation, this irradiation-induced segregation occurs at a temperature where atoms transport via irradiation-induced point defects is possible, but redistribution of solute atoms via thermal vacancies is not the dominant process. Experimentally has been determined that if the solute atoms are smaller than the solvent atoms, the solute atoms will migrate toward sinks (surfaces, grain boundaries, dislocations, etc.), and larger atoms decrease their concentration near these sinks [7].

The knowledge acquired about the basic mechanisms of the phenomena that occur during the interaction between the ion beam with the material used as a target, the knowledge acquired as a result of the damage induced by the radiation has permitted the development of new technology to manufacture materials with specific properties due at the high control that could have over the material structure [8].

The most spectacular example of the use of materials irradiation is the analysis technique known as FIB (Focused Ion Beam). The ability of this technique to grind, image, and deposit material is critically dependent on the nature of the particle-solid beam interaction.

1.1 Alloys sputtering

The material surface sputtering induced by the irradiation is explained by Sigmund's theory or with modifications of itself. The phenomenological model developed by Sigmund employs the collision cascade as the fundamental event to explain the material surface sputtering: the incident ion upon collision with the solid initiates a series of atomic collisions with the surrounding atoms in the interaction volume, these atomic collisions are denominated the collision cascade. The incident ion energy is shared among those atoms that are located within of collisions cascade and promoted atomic detachment and atomic mobility. Only those collisions that occur near of material surface are effective in ejecting atoms out of the material surface. The great majority of atoms removed come from the first atomic layers of the material surface. The sputtering yield is the average number of atoms ejected from the material surface per incident ion. The sputtering yield depends on several things: the incidence angle at which ions collide with the material surface, the incoming ions energy, ions/surface atoms mass ratio, and the material surface binding energy. At a higher number of atomic collisions that occur in a near-surface region, the surface Sputtering Yield would be higher.

The Sputtering Yields' main characteristics for complex materials as binary alloys are the same as a pure element, but there are additional complications since there are two different types of atoms in the material. The two species cannot be eroded at an equal rate due to differences in energy partitioning, being removed probability or binding energies. Experimentally, preferential sputtering of one atomic species over the other has been observed in many alloys or compounds [9].

1.2 Preferential sputtering

In the sputtering yield description of a multicomponent system, the preferential erosion influence and surface segregation must be included. For a homogeneous specimen with two components A and B, the surface concentrations, Ns, are equal to the volume concentrations, Nv, in the absence of segregation to the surface, which must occur due to thermal processes. At the sputtering onset.

$$N^s_A / N^s_B = N^v_A / N^v_B \qquad (1)$$

The partial Sputtering Yield of the atomic species A and B is defined by:
$Y_{A, B}$ = (atoms eliminated amount A, B)/incident particles.
The sputtering yield of species A, Y_A, is proportional to the surface concentration, N^s_A, and similarly, Y_B is proportional to N^s_B.
The partial sputtering yield ratio is given by:

$$Y_A / Y_B = r \left(N^s_A / N^s_B \right) \qquad (2)$$

Where the erosion factor, r, considers the differences in surface binding energies, escape depths of the ejected atoms and energy transfer within the cascade. Measured values of, r, are generally in the range 0.5–2.

On the other hand, there are several mathematical models that describe the sputtering Yield, it is important to mention that all of these models are based on the work of P. Sigmund. His work "Theory of Sputtering I. Sputter yield of Amorphous and Polycrystalline targets" published in Physical Review is a benchmark in this field [10].

1.3 Sigmund mechanism

The sputtering process nature is discontinuous due to each one ion initiating an atomic collision cascade. The sputtering yield is dependent on the deposited energy fraction at the surface, which is the function of surface topography local and ion beam incidence angle. From atomic level point of view, the surface sputtering has a random nature as a result the sputtering yield varies markedly from one event to another. These two phenomena have important consequences with respect to the surface topography when considering dimensions similar to those of atomic collision cascade.

A particularly violent event can produce a crater by removing a large number of atoms, either by erosion or by sublimation from a hot spot. The sputtering yield variation with position leads to the prediction that in the absence of a surface smoothing mechanism such as diffusion; flat surfaces are unstable, against increasing roughness at scales similar to the atomic collision cascade size. This instability can lead to the growth of small irregularities of atomic dimensions, such as surface protuberances.

2. Experimental evidence of microstructure changes induced by ion beam irradiation

In order to explain the changes induced by irradiation on a complex surface formed by the presence of two regions with different chemical compositions, the Ni-22%at.Si (Ni-22Si) concentrated alloy was selected. The Ni-22Si alloy is of the hypereutectic type, consisting of two regions, the dendritic and the interdendritic, the dendritic region is constituted by the $Ni_3Si_{-monoclinic}$ phase, and in the interdendritic region there is a regular eutectic formed by the regular alternation of the Ni(Si) and $Ni_3Si_{-monoclinic}$ phases lamellae (**Figure 1**), it was determinate by optical microscopy that 70% of the surface is occupied by the $Ni_3Si_{-monoclinic}$ phase. The terminal Ni(Si) phase has a maximum solubility of 12 atomic % of Silicon at the irradiation temperature, on the other hand, the $Ni_3Si_{-monoclinic}$ phase is an intermetallic phase with a Silicon concentration of 25 atomic %.

In summary, the main characteristics of the hypereutectic microstructure are the presence of two crystalline phases with different chemical compositions and crystalline structures, as well as the high density of grain boundaries.

Before being irradiated, the surface was mirror-polished to eliminate protrusions or surface defects that could locally modify the sputtering yield. The surface was analyzed using atomic force microscopy (AFM) to establish the surface topography parameters, an AFM image of the Ni-22Si alloy surface before being irradiated is shown in **Figure 2**.

As a result of the MFA images analysis of the surface before being irradiated, the protrusions' existence with heights of angstroms has been detected, as well as the presence of a step between the dendritic and interdendritic regions, the dendritic
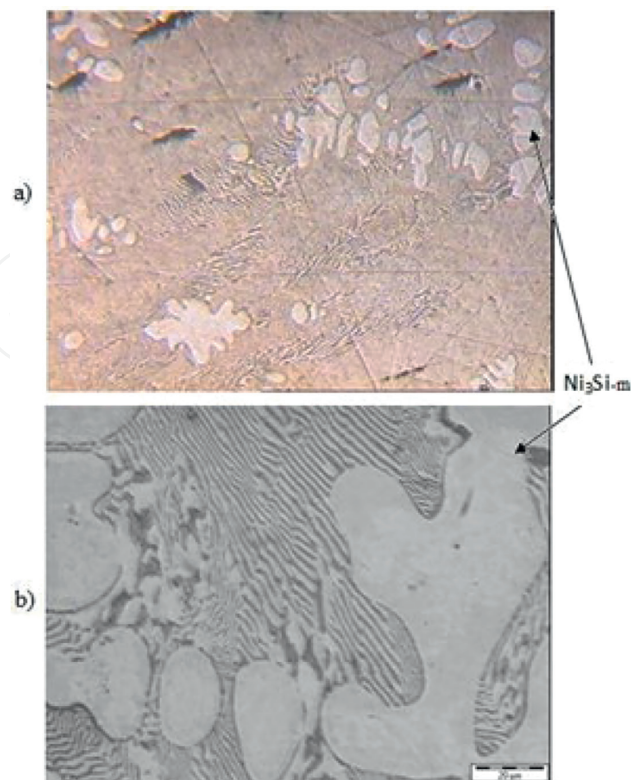
Figure 1.
Microstructure of the hypereutectic alloy (a) without chemical attack and (b) with chemical attack.
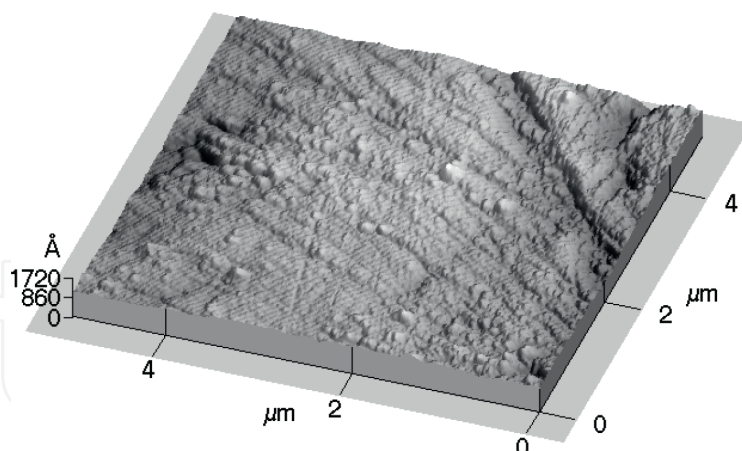
Figure 2.
Atomic force microscopy image of the Ni-22Si alloy surface before to be irradiated.

region is located on the upper right side of **Figure 2**, the interdendritic region occupies the rest of the surface shown in **Figure 2**.

2.1 Irradiation conditions

The Ni22at%Si was prepared by solidification in an inert atmosphere furnace, the alloy was templated from melting temperature to room temperature in water. The irradiation targets were obtained by electroerosion with the next geometrical characteristics: alloy circular plates with an area of 1 cm^2 and thickness of 300 μm. Prior to being irradiated the plate's thickness was reduced to 100 μm to a mirror finish by mechanical polishing. The irradiation conditions used to bombard the alloy circular plates were Ni ions beam of 3.66 MeV at 650° C, the incidence angle of the ion beam to the surface was 90°, two different ion fluence of 3.97×10^{16} and 1.99×10^{17} ions/cm^2 were used to evaluate the irradiation time effect. It was used a pyrometer focused on the irradiated area, with a tolerance of ±10°C to perform the temperature control of the irradiated area. The irradiation was performed in a Tandetron-type GIC linear accelerator, designed to provide a large flow of ions 1.9×10^{17} ions/cm^2 [11].

3. Analysis of the surface microstructure changes induced by the ion irradiation

Figure 3 shows, an optical microscopy image of the irradiated and non-irradiated regions of the Ni-22Si alloy, two regions are observed, one in bright contrast and the other one in dark contrast, the dark contrast region corresponds to the irradiated region. This change from bright to dark contrast is generated by the surface topography modification induced by irradiation, as a consequence, the reflective power of the irradiated surface is reduced. The surface topographic change is generated by the preferential sputtering of boundaries between the dendritic lobes and the interdendritic region, as well as by the crater's formation, dark spots, both changes are surface damage induced by irradiation [12].

As a result of several reported works on irradiation-induced damage in metallic alloys, it has been established that preferential sputtering of grain boundaries occurs because the atoms located in that region have lower binding energy with their neighbors [13].
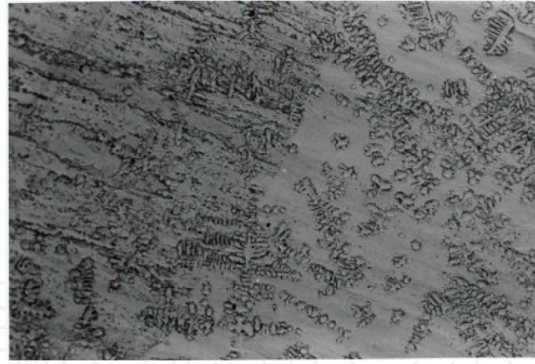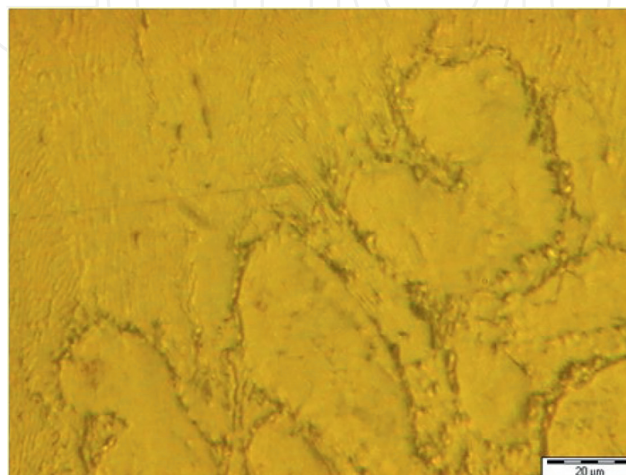
Figure 3.
*Optical microscopy image of the irradiated and non-irradiated region.*

3.1 Preferential erosion

Figure 4 shows an optical microscopy image of the boundary formed between the dendritic lobes and the interdendritic region, this image shows in detail the preferential sputtering suffered by the border between the two regions, the sputtering yield suffered by the border is greater than the erosion suffered by the dendritic region or the interdendritic region. In the image in **Figure 4**, it can also be seen that the sputtering of the boundary is not homogeneous, the alternation of protrusions and hollows is clearly observed, for this reason, atomic force microscopy was used to analyze in greater detail the sputtering process of grain frontier.
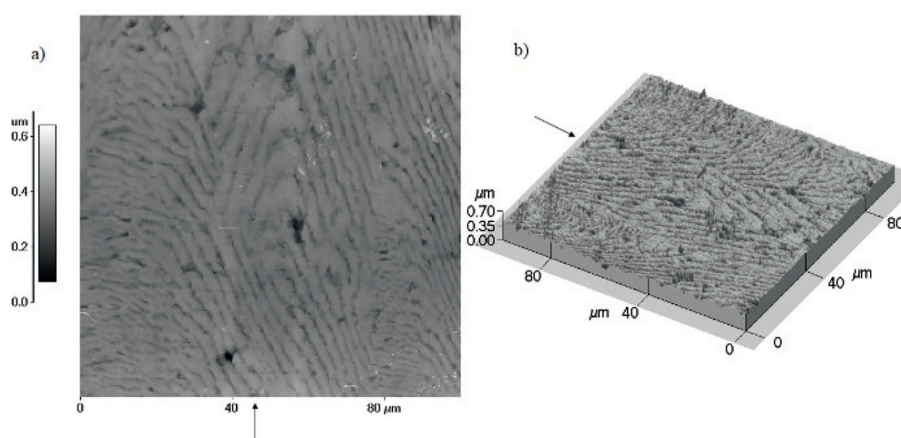
Atomic force microscopy images (**Figure 5**) of the irradiated region provide experimental evidence of sputtering process inhomogeneity, in **Figure 5(a)**, on the left side, a dendrite nodule (monophasic region) and on the right side of the same figure, the inter-dendritic region (biphasic region), and the border formed between the two regions can be seen. In **Figure 5(a)**, it is clearly seen that some specific regions of the boundary had suffered a greater sputtering giving rise to the bridges formation with a regular alternation, **Figure 5(b)** shows the same boundary at higher resolution, this last image allows us to establish that the sputtering process is indeed a non-homogeneous process since certain portions of the boundary were totally eliminated.

Figure 4.
Optical microscopy image of irradiated región.
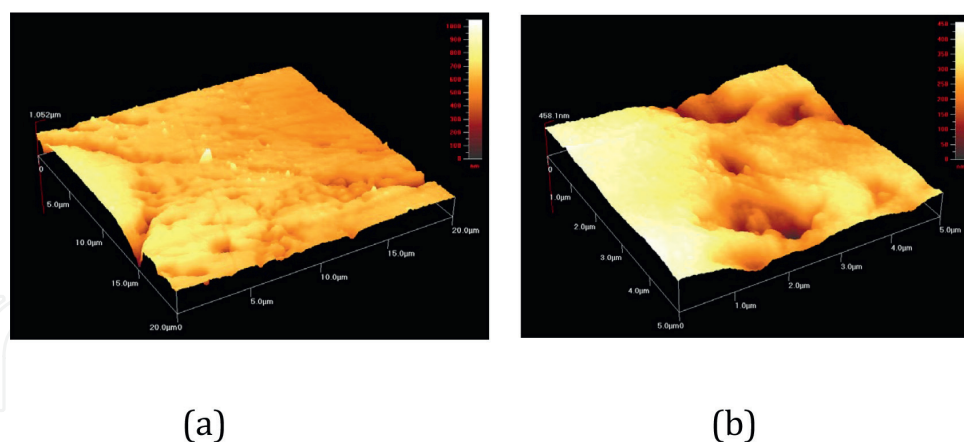
Figure 5.
Atomic force microscopy images of the boundary between dendritic and interdendritic regions.

Figure 6.
Atomic force microscopy images of the valley-ridges pattern formed in the interdendritic region because of sputtering.

Figure 6 shows atomic force microscopy images of the interdendritic region to establish the origin of the sputtering inhomogeneity. Experimental evidence provided by MFA images (**Figure 6**) of the interdendritic region shows that the valleys and ridges regular pattern was formed as a sputtering result, this pattern regularity is very similar to the phases alternation that forms the $Ni(Si)$-Ni_3Si-monoclinic regular eutectic. Therefore, it is hypothesized that one of the phases was preferentially sputtering and that this preferential sputtering is promoted by the chemical difference in composition between the two phases.

The sputtering yield of each phase that forms the $Ni(Si)$-Ni_3Si-monoclinic regular eutectic was calculated using SRIM 2013 code [14]. **Table 1** shows the results of the sputtering yield simulation at the above-mentioned irradiation conditions.

Simulation results indicate that the terminal phase $Ni(Si)$ has the highest sputtering yield. This means that this phase is the one that underwent the greatest sputtering under the irradiation conditions employed and consequently gives rise to the valleys formation observed in the atomic force microscopy images analyzed.

In addition, scanning electron microscopy images of the interdendritic region, **Figure 7**, show the same valley-ridges pattern, it should be remembered that the field depth of this microscopy is limited, however, the pattern characteristics are clearly observed.

7

Phase	Sputtering yield	Depth of maximum damage (μm)	Ion range (μm)
Ni(Si)	1.03	1.2	1.9
$Ni_3Si_{-monoclinic}$	0.81	1.3	2.0

Table 1.
Sputtering yield simulation by SRIM 2013 code [13].

(a)   (b)
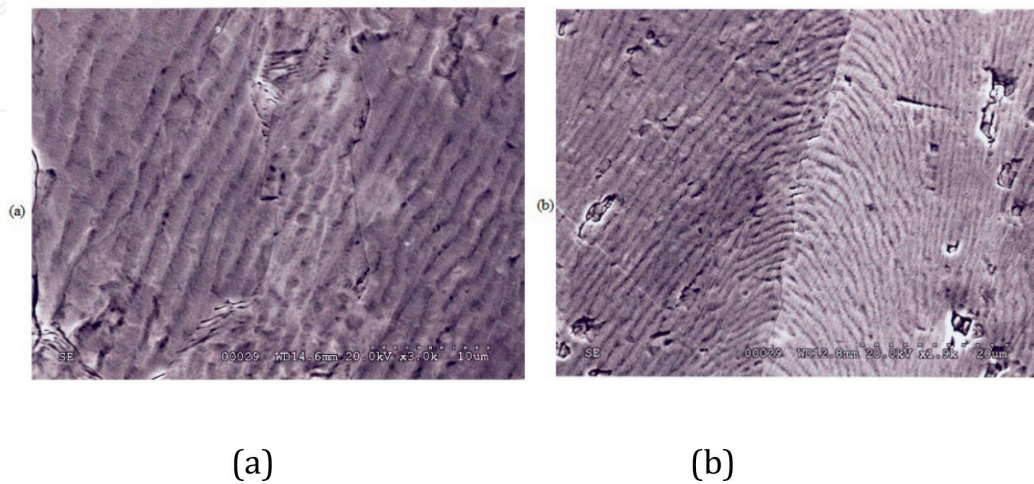
Figure 7.
Scanning electron microscopy images of the interdendritic region irradiated, (a) interdendritic region and (b) eutectic colonies.

In the images shown in **Figure 7**, in addition to the pattern of valleys and ridges, other changes generated by irradiation can be clearly seen, craters and in **Figure 7(b)** it is observed how the boundary between eutectic colonies was sputtered, which denotes the high susceptibility to the chemical composition local variation of sputtering process induced by ion beam irradiation.

## 3.2 Surface protrusions evolution under ion irradiation

Figure 2 shows an MFA image of the surface before being irradiated in which it is observed that there are protuberances with angstroms heights without a defined pattern in its surface distribution, it has been established that such protrusions as an irradiation consequence result in the peaks formation with nanometer dimensions, which can be seen in **Figure 8**.

The roughness enhancement mechanism proposed by Sigmund [15] explains the formation of these nanostructures in terms sputtering yield variation generated as a consequence of the local incidence angle change of the ion beam.

In the case of three-dimensional, cone-like protrusions, the sputtering yield is about 0.2 in the cone zones with dimensions similar to or larger than the displacement cascades size. For protrusions with dimensions of the order of displacement cascade size the sputtering yield has values < 1, although this model predicts the nanoparticle's formation from protrusions with angstrom dimensions, its major contribution is that it predicts the most important geometrical feature, the nanoparticles top will always tend to have a conical shape. As an above result and in the absence of any surface smoothing mechanism by migration, pre-existing surface protrusions on the
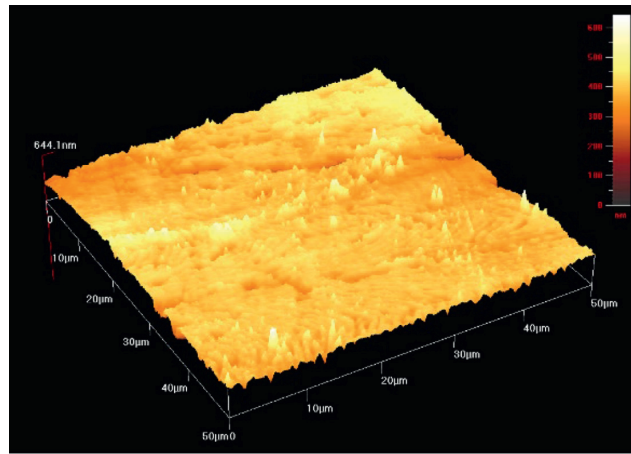
Figure 8.
Atomic force microscopy image shows a panoramic view of the interdendritic region of the irradiated zone where the distribution and size of the induced nanoparticles can be observed as a result of the interaction process of the irradiation with the protrusions observed in **Figure 2**.

(a) (b)
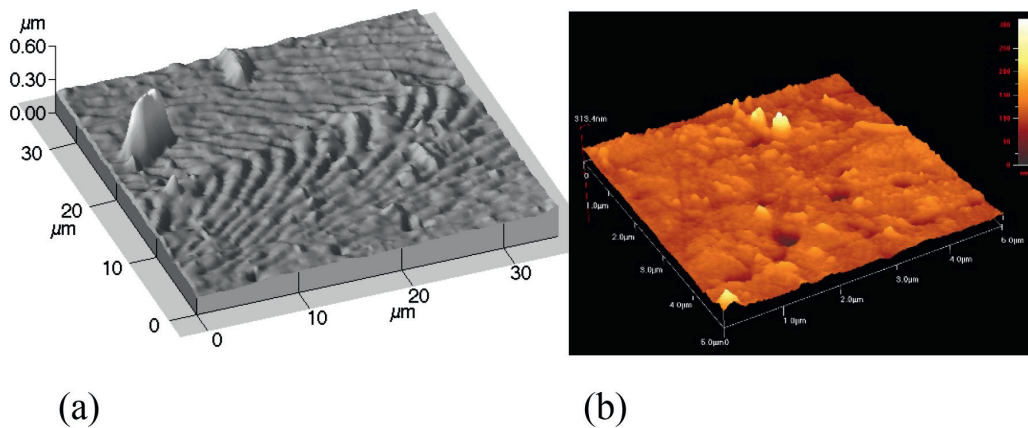
Figure 9.
Nanopicks formed in the (a) interdendritic zone and in the (b) dendrites branches.

irradiated surface will be stable and will tend to grow as a result of the sputtering yield variation promoted by the local incidence angle change.

Figure 9(a) and (b) shows MFA images of the dendritic (**Figure 9b**) and interdendritic (**Figure 9a**) regions of the irradiation-affected area, both figures show the formation of peaks, cones, and other types of geometries and all of them have peaks that tend to have a conical shape. Another important factor detected is that the sputtering originated by chemical composition is of lower intensity than the geometrical sputtering, induced by incidence angle local variations of the ion beam.

3.3 Microstructural elements effect over the sputtering yield

When analyzing the changes generated by irradiation with nickel ions in the hypereutectic microstructure of the Ni-22Si alloy (**Figure 2**), the following results were obtained, it was detected that the dendrites ($Ni_3Si_{-monoclinic}$) have a lower sputtering yield with respect to the interdendritic region.

Figure 10(a) and **(b)** shows the sputtered surface profile of two dendrites because of ion beam irradiation.

(a)

(b)

(c)

(d)
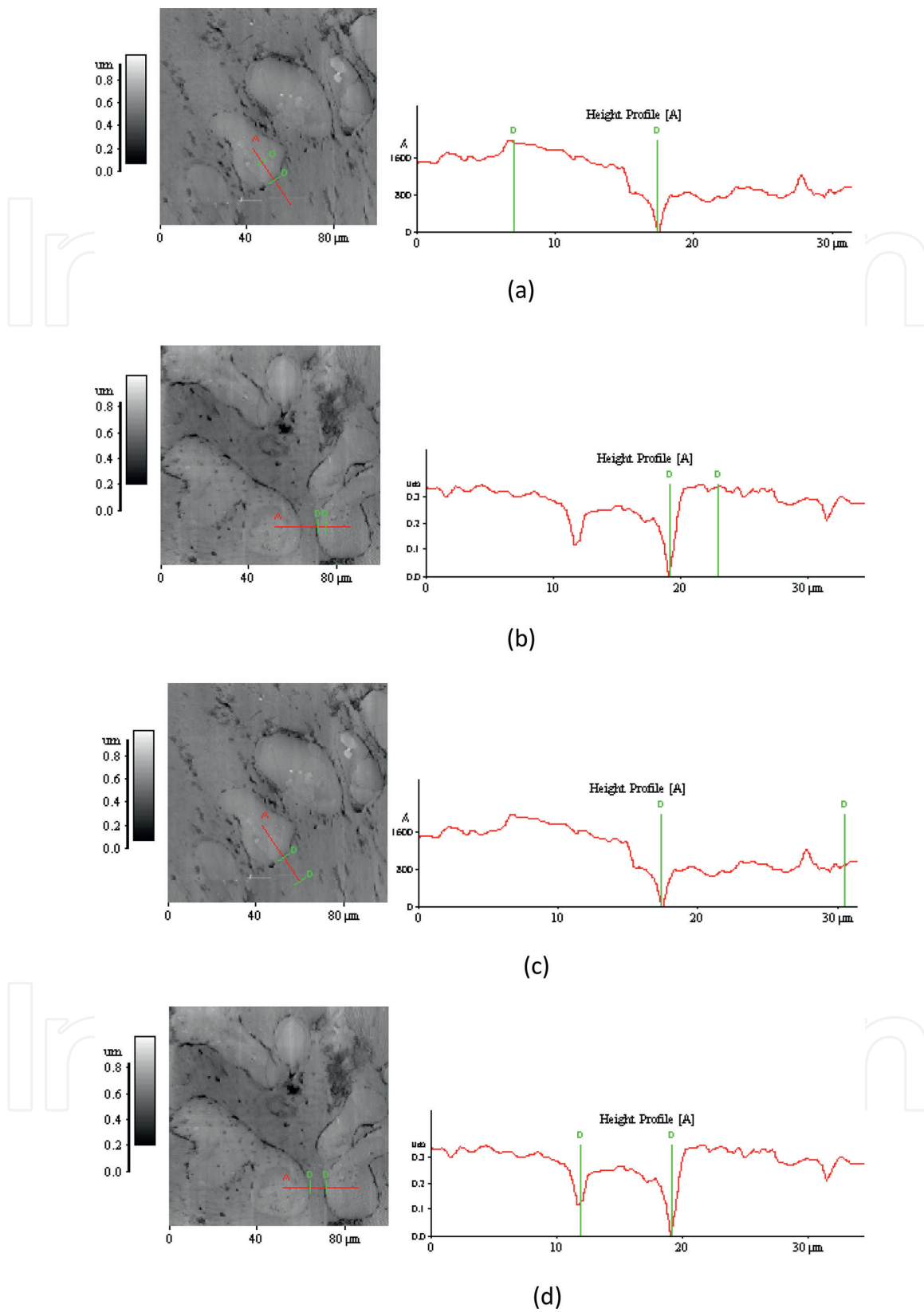
Figure 10.
Atomic force microscopy images and height profiles of the microstructural elements shown.

The regions delimited by the vertical lines are part of the dendrite(s) seen in the image to the left of the height profile, it is clearly determined that the dendrites have a lower atomic erosion ratio with respect to the interdendritic region.

Figure 10(c) presents the height profile of the interdendritic region shown in **Figure 10(a)** and clearly shows that on average the interdendritic region has a lower height with respect to the attached dendritic region, the initial surface before being irradiated did not have this type of height variations among its microstructural constituents.

On the other hand, **Figure 10(d)** shows the interdendritic region between the two dendrites shown in **Figure 10(b)**. Once again it is clearly seen that the interdendritic region has a lower height with respect to the height of both dendrites. On the other hand, there is another microstructural element in these images that must be analyzed; this is the grain boundaries and interfaces.

In conclusion, it can establish that the monophasic region, i.e., the dendrites, has a lower sputtering yield compared to the biphasic region, the interdendritic region and that because of this difference in sputtering yield, the difference in level between the dendrites and the interdendritic region is formed.

3.4 Effect of grain boundaries and interfaces on the sputtering yield

In order to analyze the grain boundaries effect on the sputtering yield, the hyper-eutectic alloy was irradiated with two doses, 80 and 380 dpa, and the grain boundaries effect was evaluated using Force Atomic Microscopy. **Figure 11** shows AFM images of the irradiated region with both regions, the height profile, and the correspondent image of the surface irradiated at both doses, the image at 80 dpa is shown in **Figure 11(a)** and the image at 380 dpa shown in **Figure 11(b)**.
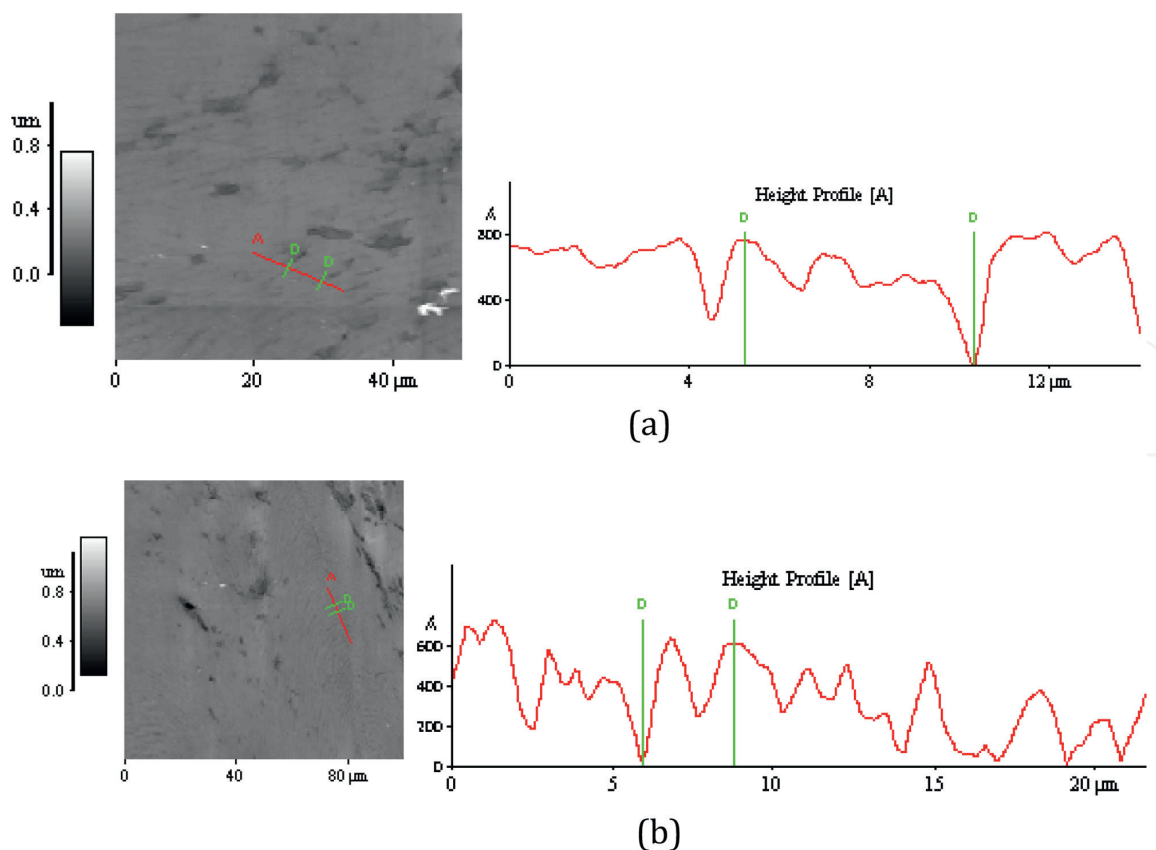
Figure 11.
Atomic force microscopy images and height profiles of microstructural elements shown irradiated, (a) at 80 dpa and (b) at 380 dpa.

| Región	Roughness (nm)			Región characteristic:
	Non-irradiated	Irradiated with 80 dpa	Irradiated with 380 dpa	
Dendrític	70.5	215	261	Monophasic
Ínterdendrític	70.5	322	192	Biphasic

Table 2.
Roughness of dendritic and interdendritic regions.

Table 2 shows the results of roughness measurements carried out to evaluate the changes induced by the irradiation dose increase on the lamellae morphology of Ni(Si) and Ni$_3$Si$_{-monoclinic}$ phases.

Results analysis shows that the roughness increase rate in the dendritic region is a dose function, an expected result based on the mathematical models of sputtering yield [16]. However, the roughness rate change in the interdendritic region shows a pronounced increase at a dose of 80 dpa, behavior that denotes the effect of Ni(Si) phase preferential erosion, but at a dose of 380 dpa the roughness value decreases markedly. This could be caused by a smoothing mechanism generated by mass transport as a consequence of the irradiation temperature, in order to determine the nature of this surface smoothing mechanism, the geometric factors of the pattern of valleys and ridges generated in the interdendritic region were measured.

Measurements of interdendritic regions' height profiles show a significant change pattern geometry of valleys and ridges formed in that region due to the preferential sputtering generated by the chemical composition of the phases that form the regular eutectic. **Figure 12** shows the diagram of the valley-ridges pattern, as well as the comparative height profile of the dendritic and interdendritic regions at both irradiation doses. **Table 3** shows the average results of the valley- ridges pattern geometric characteristics at both irradiation doses.

When analyzing the results of **Table 3** in conjunction with **Figure 12**, it is concluded that with increasing irradiation dose an additional sputtering mechanism with a geometrical character is present and it is this mechanism that is responsible for irradiated smoothing surface at a dose of 380 dpa. The theoretical foundation of this geometric erosion mechanism was provided by the erosion mechanism proposed by Sigmund [16].
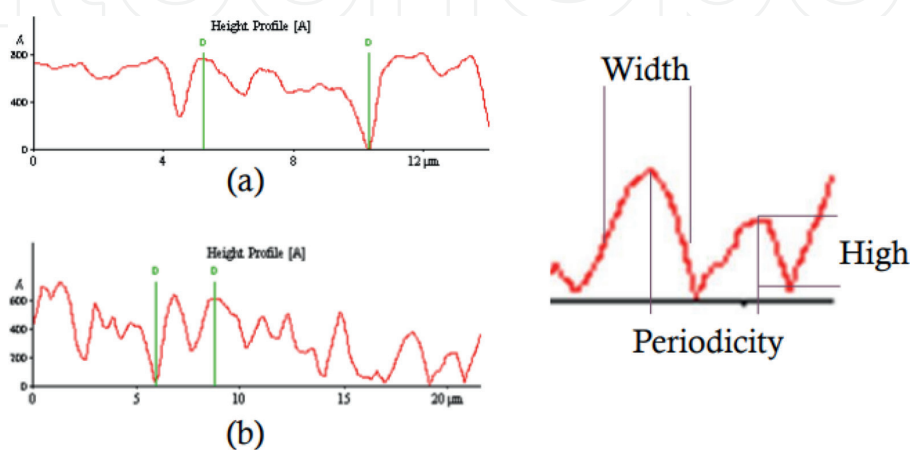
Figure 12.
The valleys and ridges regular pattern diagram, and height profiles at both doses, (a) 80 dpa and (b) 380 dpa.

Dosis (dpa)	80	380
Ridges width (µm)	2.27	1.41
Ridges height (Å)	393	224
Periodicity (µm)	1.2	1

Table 3.
Geometric characteristics of the valleys and ridges regular pattern as a function of irradiation dose.

In conclusion, the interfaces considerably increase the sputtering yield until the ion beam incidence angle reaches a certain critical value at which, the geometric sputtering mechanism is greater than any other sputtering mechanism, and this geometric sputtering promoted the irradiated surface smoothing by a non-diffusional mechanism.

The increased of interdendritic region sputtering yield generated by increased sputtering yield due to grain boundaries sputtering plus interdendritic region sputtering by geometric mechanism promoted the formation of an unevenness between the dendritic and interdendritic region.

4. Surface sputtering applications

The material sputtering as a result of being irradiated with some irradiation type has a large number of practical applications, for example, in thin film deposition and as a material characterization tool. A series of images of the fabrication process of a sample in cross-section for transmission electron microscopy are shown in **Figure 13**. The sample was obtained using a (Focused Ion Beam system) dual beam scanning microscope, this type of microscope has two optical systems, one of electrons and the second of ions, with both systems, it is possible to obtain images with different perspectives. The cutting process is performed by sputtering the selected region using a gallium ion beam.

Figures 13 and **14** show images of the sample selection and cutting processes, both of which are very high-precision processes. The sample sizing process is performed using sputtering of the excess material, depending on the dimensions of the selected

(a)   (b)
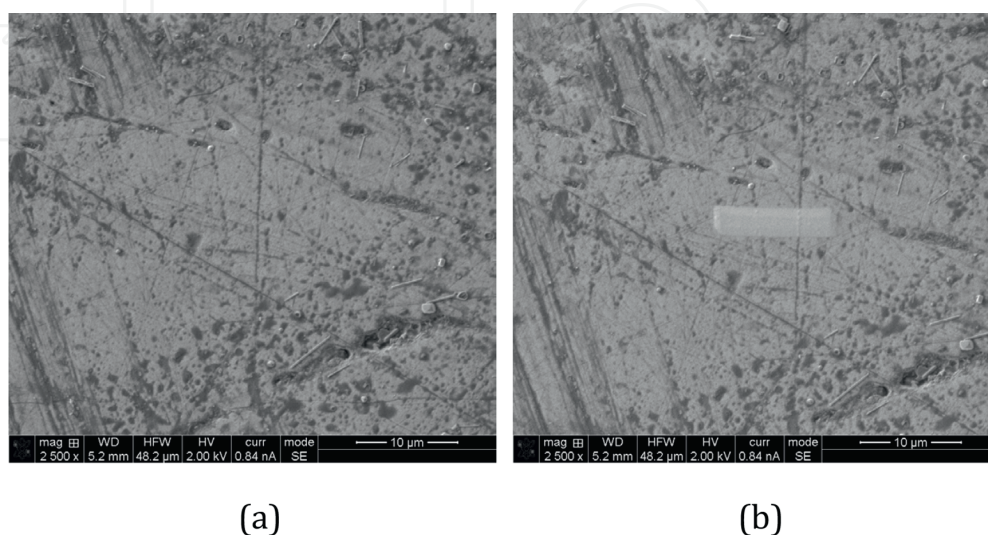
Figure 13.
The first stage consists of selecting the area from which the sample is required, (a) sampling area and (b) selected sample.

(a)　　　　　　　　　　　　　　　　(b)

(c)　　　　　　　　　(d)
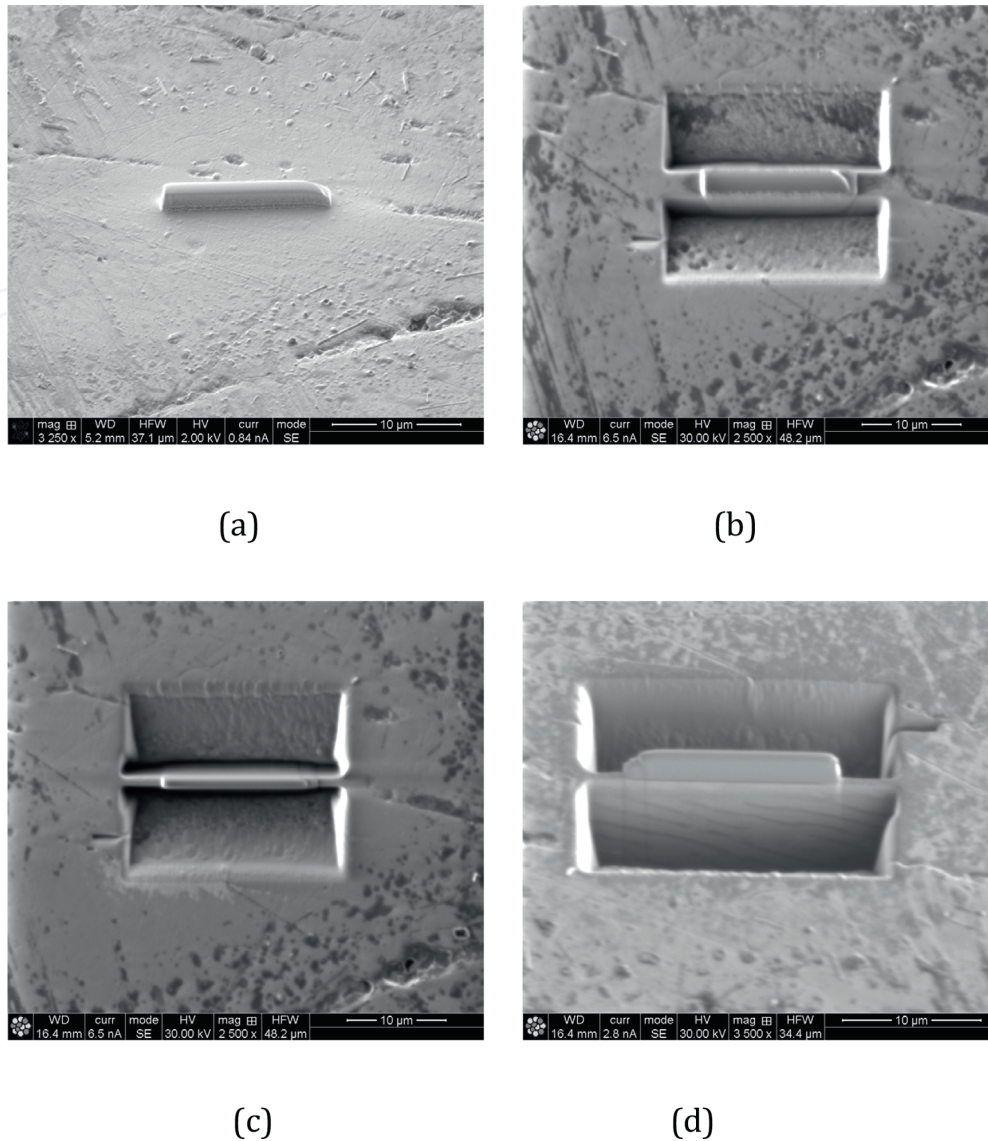
Figure 14.
Shows images of the sizing process of the selected sample, (a) sample, (b) cuts to limit the sample, (c) delimitation of the depth and (d) sample ready to be extracted.

area the removal process takes minutes, and the material removed by the sputtering process is evacuated from the chamber via the vacuum system of the microscope. This sizing system can be used on a wide range of materials without causing contamination or modification of the sample microstructure.
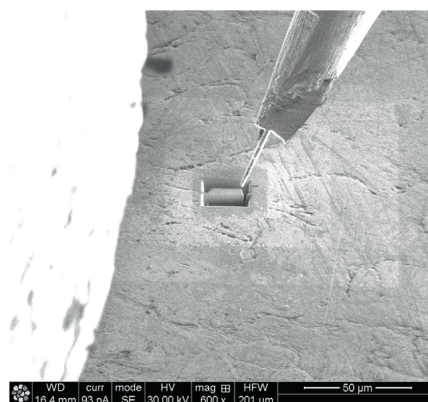
Figure 15 shows a series of images of the sample extraction process, as well as the preliminary cuts, welding of the sample with the extraction needle and the extraction process, these steps are very delicate because the sample can be lost in case of hitting the wall of the groove from which it is extracted.

The last stage of the process consists of transferring the sample to a sample holder where the thickness of the sample will be reduced via sputtering to a thickness of 100 nm. **Figure 16** shows the image of the sample placed in the sample holder.
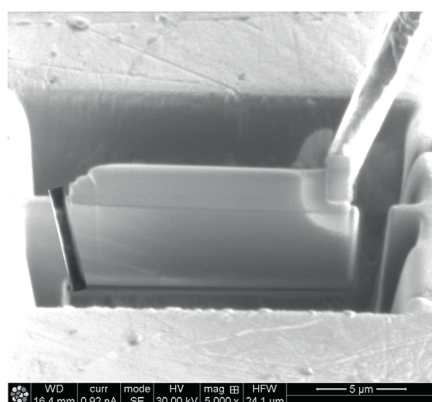
This sampling process allows obtaining samples with very high precision and relatively very fast, which is a consequence of the high spatial resolution of sputtering, which is determined by the precision with which the beam diameter is controlled.
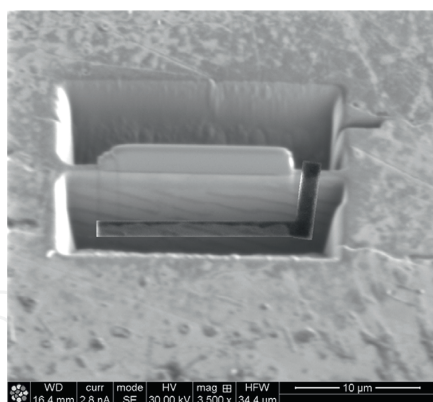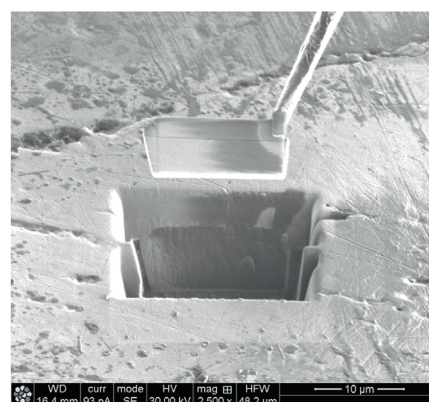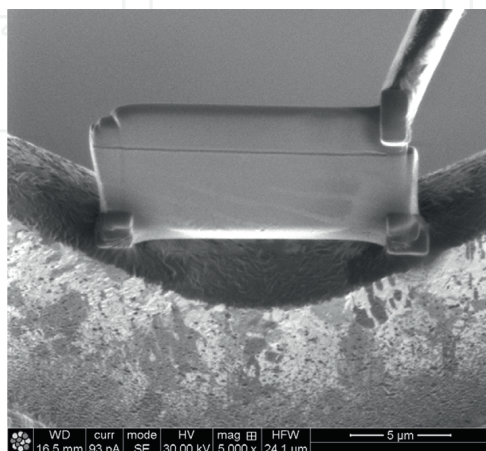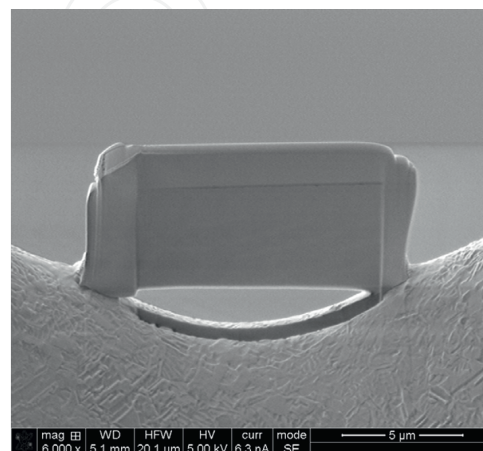
(a) (b)

(C) (d)

Figure 15.
Shows images of the sample extraction process, (a) preparation cuts, (b) approach of the extraction needle, (c) joining of the extraction needle and sample via soldering and (d) sample extraction.

(a) (b)

Figure 16.
Images of the process of mounting the sample in the sample holder to reduce its thickness to about 100 nm.

15

5. Conclusion

The microstructure changes induced by ion beam irradiation of the irradiated surface depend on the parameters associated with the ion beam, ion type, beam flux, beam energy, and irradiation time, as well as on the surface microstructure, mainly on the phase's chemical composition, the phases distribution on the surface, the surface defects present and the ion beam-surface interaction parameters, mainly the ion beam incidence angle and the mass ratio between target and the ion used to irradiate the material.

As a result of the ion beam—Surface interaction process, several sputtering mechanisms are activated, mainly the chemical one, giving rise to the preferential sputtering of one of the phases present on the surface, the terminal phase Ni(Si) was determined to be preferentially eroded, since it has the highest sputtering yield (see **Table 1**), also when comparing its average molecular weight with the atomic weight of Nickel it is observed that the difference between both is less than 10%, which promotes a greater energy transfer to this phase. On the other hand, it is known that there is a critical local angle of incidence of the ion beam that promotes the activation of the geometric sputtering process, the main characteristic of this geometric mechanism is that it has the potential to modify the topography generated as a result of the preferential erosion of a specific microstructural component, even in an extreme case to produce the smoothing of the surface under irradiation.

Finally, the degree of the changes induced on the irradiated surface are strongly linked to the complexity of the microstructure of the surface of the material used as a target, therefore, the use of sputtering as a tool to develop new materials is conditioned to the microstructural characteristics of the material to be used as target and to the type of ion employed.

Glossary

Atoms implantation: Procedure that consists of incorporating atoms other than that of the base material to modify its characteristic properties.

Crystal lattice: A scheme by which crystal structures are classified according to unit cell geometry. This geometry is specified in terms of the relationships between edge lengths and interaxial angles.

Diffusion: Atoms moving and changing places, i.e., directed or undirected mass transport by atomic motion. Atomic diffusion in solids is far slower than in gases or liquids.

Dislocation: A linear crystalline defect around which there is atomic misalignment. Plastic deformation corresponds to the motion of dislocations in response to an application.

Grain boundaries: The interface separating two adjoining grains having different crystallographic orientations.

Microstructure: The structural features of an alloy (e.g., grain and phase structure) that are subject to observation under a microscope.

Nanostructures: Structure with one or more dimensions at the nanoscale.

Polycrystalline: Refers to crystalline materials that are composed of more than one crystal or grain.

Roughness: is the degree of unevenness of a solid surface below the size scale of its shape or waviness, but above the irregularity of crystal lattice structures. The roughness has an influence on the wettability of a solid.

Segregation: Enrichment of solutes in grains and grain boundaries. An approximation to the segregation tendency of a solute in grain and grain boundary is its apparent solubility: the lower the apparent solubility, the higher the enrichment factor of that element in grain and grain boundary.

Shear stress: The instantaneous applied shear load divided by the original cross-sectional area across which it is applied.

Sputtering: A phenomenon in which microscopic particles of a solid material are ejected from its surface after the material is itself bombarded by energetic particles of a plasma or gas.

Author details

Carlos A. Camacho Olguín[1]*, Arturo García Bórquez[2],
Carlos A. González Rodríguez[1,3], Héctor Cruz Mejía[1,3] and Marco Solorio Ávila[1]

1 Polytechnic University of the Valley of Mexico, Tultitlan, State of Mexico, Mexico

2 National Polytechnic Institute, Mexico City, Mexico

3 National Autonomous University of Mexico, Mexico City, Mexico

*Address all correspondence to: cachisolguin@hotmail.com

IntechOpen

References

[1] Dey S, Dutta AN, Gayathri, Mukherjee PK, Tapatee KR. Characterization of ioninduced microstructural changes in oxygen irradiated Ti–6Al–4V. Radiation Effects and Defects in Solids. 14 Jul 2022;**177**(9-10):972-991. DOI: 10.1080/10420150.2022.2098748

[2] Cui M, Jin P, Shen T, Zhu Y, Pang L, Wang Z, et al. Microstructure change, Nano-Hardness and Surface Modification of CN-G01 Beryllium Induced by Helium Ions. Metals (Basel) [Internet]. 2022;**13**(1):60. Available from: https://www.mdpi.com/2075-4701/13/1/60

[3] Luneville L, Garcia P, Simeone D. Predicting nonequilibrium patterns beyond thermodynamic concepts: Application to radiation-induced microstructures. Physical Review Letters. 2020;**124**(8):085701. DOI: 10.1103/PhysRevLett.124.085701

[4] Camacho-Olguín CA, Garcia-Borquez A, Paz del Angel V, Fuente JAM-DL, González-Rodríguez CA, Ramos-Tercero LM, et al. Formation of the $Ni_{31}Si_{12}$ phase induced by the irradiation of nickel ions on the eutectic α-Ni-Ni_3Si-monoclinic, with a 380 dpa dose. Radiat Eff Defects Solids. 2020;**175**(9-10):925-937. DOI: 10.1080/10420150.2020.1793338

[5] Yano KH, Kohnert AA, Kaspar TC, Taylor SD, Spurgeon SR, Kim H, et al. Dose rate dependent cation & anion radiation enhanced diffusion in hematite. J Mater Chem A Mater Energy Sustain [Internet]. 2022;**10**(45):24167-77. Available from: https://pubs.rsc.org/en/content/articlehtml/2022/ta/d2ta03403d

[6] Belkacemi LT, Meslin E, Crocombette J-P, Radiguet B, Leprêtre F, Décamps B. Striking effect of solute elements (Mn, Ni) on radiation-induced segregation/precipitation in iron-based model alloys. Journal of Nuclear Materials. 2021;**548**:152807

[7] Jiang W, Kovarik L, Zhu Z, Varga T, Bowden ME, Matthews BE, et al. Microstructural evolution and precipitation in γ-LiAlO2 during ion irradiation. Journal of Applied Physics. 2022;**131**(21):215902

[8] Li W, Zhan X, Song X, Si S, Chen R, Liu J, et al. A review of recent applications of ion beam techniques on nanomaterial surface modification: Design of nanostructures and energy harvesting. Small. 2019;**15**(31):e1901820. DOI: 10.1002/smll.201901820

[9] Nastasi M, Mayer JW, Hirvonen JK. Cambridge solid state science series: Ion-solid interactions: Fundamentals and applications: Fundamentals and Applications. Cambridge, England: Cambridge University Press; 1996

[10] Sigmund P. Theory of sputtering. I. sputtering yield of amorphous and polycrystalline targets. Phys Rev [Internet]. 1969;**184**(2):383-416. DOI: 10.1103/physrev.184.383

[11] Camacho-Olguín CA, Rodriguez-Diaz RA, García-Borquez A, Cruz-Mejía H, Camacho-Olguín R. Effect of the energy density deposited by a 3.66-MeV Nickel ion beam on the sputtering yield of a hypereutectic alloy. Radiat Eff Defects Solids. 2022;**177**(9-10):1033-1048. DOI: 10.1080/10420150.2022.2105215

[12] Koslowski HR, Schmitz J, Linsmeier C. Segregation, and preferential sputtering of Cr in WCrY

smart alloy. Nucl Mater Energy. 2020;**22**(100736):100736. Available from: https://www.sciencedirect.com/science/article/pii/S2352179120300120

[13] Barr CM, Chen EY, Nathaniel JE II, Lu P, Adams DP, Dingreville R, et al. Irradiation-induced grain boundary facet motion: In situ observations and atomic-scale mechanisms. Science Advances. 2022;**8**(23). DOI: 10.1126/sciadv.abn0900

[14] SRIM-2013 Manual and Code. Available from: http://www.SRIM.org

[15] Simeone D, Garcia P, Luneville L. Radiation-induced patterning at the nanometric scale: A phase field approach. Materials (Basel). 2022;**15**(9):2991. DOI: 10.3390/ma15092991

[16] Cupak C, Szabo PS, Biber H, Stadlmayr R, Grave C, Fellinger M, et al. Sputter yields of rough surfaces: Importance of the mean surface inclination angle from nano- to microscopic rough regimes. Applied Surface Science. 2021;**570**:151204. DOI: 10.1016/j.apsusc.2021.151204